Intelligent airborne monitoring of man-made marine objects using Machine Learning techniques - Part I

The objective of this study is to create a new platform for the automated detection of irregularly shaped man-made marine objects (ISMMMOs) in large datasets derived from marine aerial survey imagery. We present here the first part of the paper. The concluding part of the paper will be published in the next issue

Kaya Kuru
School of Engineering and Computing, University of Central Lancashire, Fylde Rd, Preston, Lancashire, PR12HE, UK

Stuart Clough [1]
APEM Inc., 2603 NW 13th Street, 402, Gainesville, FL 32609-2835, USA

Darren Ansell
School of Engineering and Computing, University of Central Lancashire, Fylde Rd, Preston, Lancashire, PR12HE, UK

John McCarthy [2]
APEM Ltd., The Embankment Business Park, Stockport SK4 3GN, UK

Stephanie McGovern [2]
APEM Ltd., The Embankment Business Park, Stockport SK4 3GN, UK

Abstract

The marine economy has historically been highly diversified and prolific due to the fact that the Earth's oceans comprise two-thirds of its total surface area. As technology advances, leading enterprises and ecological organisations are building and mobilising new devices supported by cutting-edge marine mechatronics solutions to explore and harness this challenging environment. Automated tracking of these types of industries and the marine life around them can help us figure out what's causing the current changes in species numbers, predict what could happen in the future, and create the right policies to help reduce the environmental impact and make the planet more sustainable. The objective of this study is to create a new platform for the automated detection of irregularly shaped man-made marine objects (ISMMMOs) in large datasets derived from marine aerial survey imagery. In this context, a novel nonparametric methodology, which harbours several hybrid statistical Machine Learning (ML) methods, was developed to automatically segment ISMMMOs on the sea surface in large surveys. This methodology was validated on a wide range of marine domains, providing robust empirical proof of concept.

This approach enables the detection of ISMMMOs automatically, without any prior training, with accuracy (*ACC*), Matthews correlation coefficient (*MCC*), negative predictive value (*NPV*), positive predictive value (*PPV*), specificity (*Sp*) and sensitivity (*Se*) over 0.95. The outlined methodology can be utilised for a variety of purposes, but it's especially useful for researchers and policymakers who want to keep an eye on how the maritime industry is deploying and make sure the right policies are in place to meet regulatory and legal requirements to promote maritime tech innovation and shape what the future looks like for the marine ecosystem. For the first time in the literature, a method, the so-called ISMMMOD, has been developed to automate the detection of all types of ISMMMOs by statistical ML techniques that require no prior training, which will pioneer the monitoring of human footprint in the marine ecosystem.

1. Introduction

The process of marine spatial planning is highly contentious due to the presence of multiple stakeholders, often with conflicting objectives and values (Elrick-Barr et al., 2022). The maritime economy has historically been highly diversified

and prolific due to the fact that the Earth's oceans comprise two-thirds of its total surface area. As technology advances, leading enterprises and ecological organisations are building and mobilising new devices supported by cutting-edge marine mechatronics solutions (Shi et al., 2017) within the framework of Automation of Everything (AoE) (Kuru and Yetgin, 2019) to explore and harness this challenging environment. More specifically, robotic vehicles, autonomous vehicles, and surface vessels have been deployed for the offshore industries and deep sea archaeology, ocean engineering projects, rescue operations and environmental measurements for the last several decades. For instance, the Argo program, an international collaboration, has deployed approximately 3900 instruments in the world's oceans to facilitate the collection of data for climatological and oceanographic studies. (Riser et al., 2016). Besides, artificial structures such as gas, oil and deep seabed mining platforms, offshore renewable energy harvesting technologies such as oil and gas installations, wind farms and wave energy converters, fish farms, ships, boats and yachts for transportation, autonomous marine vehicles from unmanned ships to smaller vessels are becoming inevitable components of the offshore environment. For instance, in recent years, the offshore wind industry has seen a remarkable expansion, with an annual rate of growth of 25%, for constructing offshore energy islands to meet the reduction of gas emission targets (Zhang et al., 2021). These may conflict with nature conservation objectives, such as habitat loss or species endangerment. In other words, this rapidly expanding industry, which allows for extensive, ongoing human influence in the marine domain, has the potential to have a significant impact on the marine environment, particularly on the marine floor, on turtles, fish, and birds. For instance, the population of monitored seabirds, which account for about 19% of the all seabird populations, declined by almost 70% from 1950 to 2010 (Paleczny et al., 2015), resulting in a net loss of almost 3 billion (%29) birds since 1970 (Rosenberg et al.,

2019). The decline of bird populations serves as a stark reminder of the need for immediate action to mitigate threats to the eventual decline of avifauna and the resulting degradation of ecosystem health, functionality, and services (Rosenberg et al., 2019). Intervention into nature is a natural consequence of human activities, however, when managed effectively, these interventions can be beneficial not only to the environment, but also to the ongoing development of civilisation (S`anchez-Marr`e et al., 2004). To better understand the planet and to ensure effective conservation planning, it is essential to have a comprehensive understanding of the species, habitats, and sites that require protection. Unfortunately, for the majority of species and regions, comprehensive quantitative knowledge is not yet available (Bibby et al., 1998). One of the key objectives of the development and utilisation of ecological models and applications is to influence the ecological policy practices, outputs and results in a beneficial manner (McIntosh et al., 2011). There is an urgent need to monitor the environmental upheavals, impacts and possible trends with environmental time series analysis, models and tools as the footprint of human activities increases with the rapid development of the industry. In this manner, modelling, automated detection, location and real-time monitoring of industrial sites and ecosystems around them can help uncover the current and potential future effects on nature. Furthermore, the insights observed and models developed based on these insights may help researchers and policymakers to monitor this diverse ecosystem along with the associated maritime industries and thereby help to determine the legal and regulatory requirements for reducing the ecological foot-print concerning immediate foreseeable environmental problems.

There are numerous studies in the literature to detect underwater man-made objects (MMOs) within a limited region of interest (RoI) using underwater imagery, robots or sonography. For instance, Abu et al. (Abu and Diamant, 2022) proposes a contour-based features analysis method to

discern underwater MMOs from natural environment considering that contours of MMOs' are supposed to be smoother than natural objects. There are a limited number of studies in the literature to detect specific types of surface marine MMOs using supervised Machine Learning (ML) and Deep Learning (DL) approaches that require prior training in the marine ecosystem. For instance, Han et al. (Han et al., 2022) proposed a DL technique titled LCSE-ResNet to detect, classify and locate vessels and oil platforms based on remote optical imagery, by which all other MMOs are excluded. There are no studies in the literature that investigates the detection of all types of surface marine MMOs, which makes this research the first study of its kind. Most irregularly shaped man-made marine objects (ISMMMOs) are made of materials such as metal, treated wood, fibreglass, PVC plastic, glass, or concrete and they have different types of irregular shapes and colours. Hence, it is infeasible to apply: i) a template matching technique based on a specific object to input as a template, and ii) a supervised ML approach based on a prior knowledge/similar datasets to train similar objects and then detect these objects automatically. Moreover, the current clustering algorithms used to group visual datasets are not capable of accomplishing this task with a high degree of precision (Kuru et al., 2013; Kuru and Khan, 2018), particularly for objects with indefinite shapes. Therefore, a new method is needed to realise this objective. On one hand, automatic detection of ISMMMOs is not easy based on two main reasons which pose a considerable challenge: i) the rapidly changing background depending on the camera, water turbidity, weather, wind, wave speed and period, sun glint and density of clouds, and ii) various non-definitive morphologies of MMOs. On the other hand, the characteristics of ISMMMOs differ from the natural environment and other natural objects within this ecosystem regarding the composition, features of the surface, saturation of light and colourfulness relative to the brightness to which an area radiate a varying amount of light.

Many studies aim to detect marine natural objects in sea areas using stationary land-based fixed cameras, in particular, sea animals: detection of animals in deep-sea video (Mehrnejad et al., 2013), detection of sharks using multispectral imaging (Lopez et al., 2014), and detection of killer whales using infrared spectrum (Graber, 2011). Furthermore, aerial surveys from a helicopter or small aircraft have been conducted for many years to detect, locate and monitor specific marine animals using human-based visual observations. Although there are several studies for the detection of MMOs such as ship (Saur et al., 2011), specific objects (e.g., boats, humans) on the ocean surface using infrared cameras (Leira et al., 2015). To the best of our understanding, there is no study that aims to detect all kinds of ISMMMOs automatically with unsupervised approaches using standard advanced cameras and aerial surveys, in particular, from the perspective of ecology. Aerial surveys provide a cost-effective way to collect environmental information over large areas in a short amount of time; however, they may not provide reliable data if not conducted correctly (Davis et al., 2022). Long-term data using standardised and well-structured approaches are the best way to measure change in ecology; unfortunately, this data is not available for most biogeographical regions (Clements and Robinson, 2022) due to the cost of data processing with intensive human intervention. In this sense, this study mainly aims to fill this gap in the scientific literature either by processing the collected data in an automated way, with no human intervention, to separate several hundreds of ISMMMOs from large surveys, or by processing images as they are streamed from the airborne camera systems to monitor ISMMMOs with their geospatial locations immediately with a novel approach using statistical ML techniques and HSV colour mode.

In a conventional marine survey program, there may be a large number of images, e.g., around a million, collected over a period of one year to be analysed for a particular site, and it is labour-intensive

to categorise the data into two groups: positive images containing man-made material and negative images without man-made material. In fact, many of the surveys that APEM Ltd.[3] has acquired indicate that 95% of the aerial survey images do not accommodate any targeted object (Kuru et al., 2023). According to some research on visual perception, humans perceive only a small portion of an environment or scene in detail under typical viewing conditions (Noe et al., 2000), which may result in discarding other details that should be taken into account. Although the elements that influence how a scene is perceived are not yet known, it appears that focus is a significant factor (Noe et al., 2000). Within this context, detection of ISMMMOs in large-scale images within very large surveys is a non-trivial task and labour-intensive. Therefore, the utilisation of automated intelligent computer systems to automate this work would be highly advantageous in order to facilitate the development of efficient environmental models with real-world inputs.

To the best of our knowledge, this study, for the first time, explicitly investigates the automatic detection of offshore ISMMMOs to assist researchers, environmentalists, and policymakers in monitoring and managing the various applications of the maritime industry and to provide guidance on the necessary regulations and legal requirements.

In order to illustrate the novelty of this research, specific contributions are listed below.

1. A novel methodology, the so-called ISMMMOD, that detects and splits ISMMMOs automatically in large-scale images in typical very large marine surveys is built.
2. The ISMMMOD is developed using the HSV colour space and statistical analysis of histograms of the channels in this space based on the ROC (receiver operating characteristic) curve analysis. The techniques in the methodology differ man-made-built structures from natural maritime habitats (i.e., waves, sea animals,
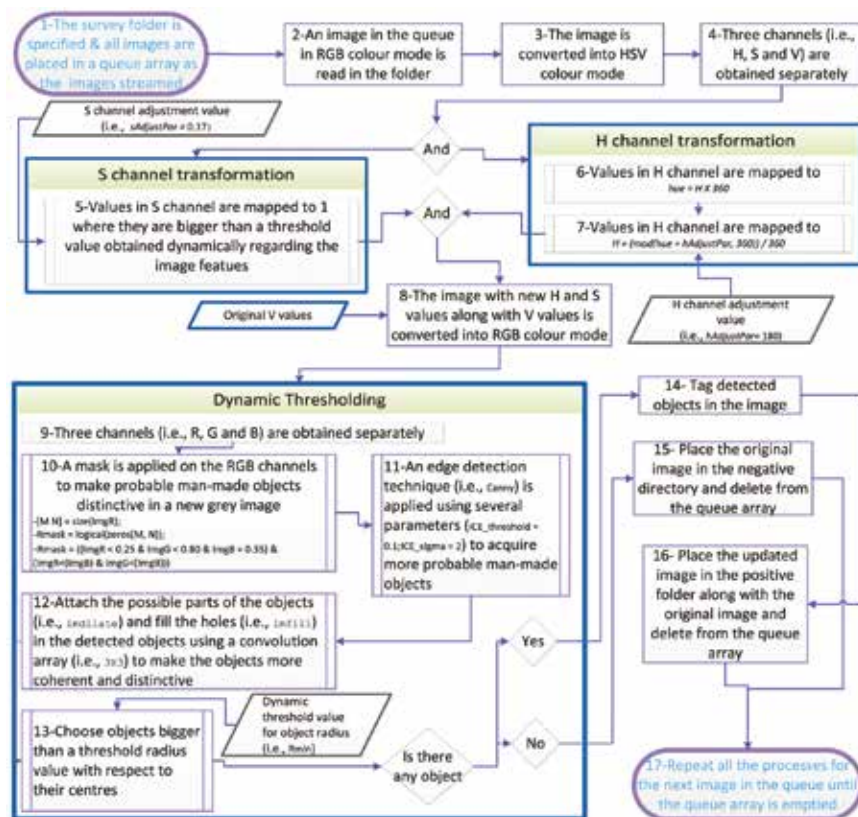

Fig. 1. Overall methodology. The images as they stream are automatically placed in the queue array to be processed in an automated way.

birds, seawater) in various aspects, in particular, composition, features of the surface and saturation of light.

The rest of this document is structured as follows: The methodology is revealed in Section 2. The datasets on which the methodology is built and tested are explored in Section 3. A summary of the findings is provided in Section 4. Discussions are outlined in Section 5. Section 6 draws a conclusion as well as future potential works. Finally, the limitations of the study are disclosed in Section 7.

2. Methodology

All types of mobile and stationary human activities – human foot-print – are required to be monitored on a regular basis and most of these activities involve the use of non-uniform, human built structures in multiple shapes during the exploration and exploitation of these tough marine ecosystem. Detecting these non-uniform structures on their highly dynamic background entails the development of a new technique that is not based on pretrained uniform object classifiers, but based on the features independent from their shapes. In this respect, we would like to reveal the features that are different from the maritime ecosystem by which a new detection method is aimed to be developed. Built structures differ from the natural maritime habitats and their creatures in various aspects, in particular, composition, features of the surface and saturation of light. The saturation level of ISMMMOs significantly varies from their surroundings (i.e., waves, sea

animals, birds, seawater). More explicitly, the saturation level of these ISMMMOs is more intense than that of the natural marine life, and in this study, more saturated sections in images considering this distinguishing feature are made distinct to detect these artificial objects. More specifically, the methodology is based on the HSV colour space (elaborated in Section 2.1) and statistical analysis of histograms of the channels in this space (elaborated in Section 2.2). The essential phases of the technique and its automated execution are depicted in *Fig. 1*. The dynamic thresholding in the implementation of the methodology is presented in Algorithm 1 and the automated implementation of the overall methodology is presented in Algorithms 2 and 3 which are placed in *Appendix A*. The execution of the methodology is exemplified for the images in Figs. 11a, 12a, 13a, 14a, 15a. The techniques in this research was built with Matlab R2020a. The interface is shown in *Fig. 2*. Generally speaking, in the proposed approach, the aerial image in RGB colour space is converted into HSV colour space and then the converted image is split into three components (i.e., channels), namely *H, S* and *V* that are designed to approximate the human vision. The result is a 3D matrix with elements of Hue, Saturation and Value. In the next step, the histograms of these components are computed as illustrated in the first rows of Figs. 11b, 12b, 13b, 14b, 15b. Then, the dynamically calculated threshold value is applied to *S* component along with shifting the *H* channel. At the end, the morphological operations, namely, masking, filter, and smoothing are carried out to extract the required area by

suppressing the irrelevant parts mentioned in Section 2.3 such as glinting regions. The statistical terms used throughout the paper are explained regarding the scope of this paper in Table 3 for the readers who are not familiar with these commonly used terms for the statistical analysis related to the confusion matrix.

Before revealing the methodology on data samples in detail, we would like to explore the basic concepts of the HSV colour space in Section 2.1 to shed light on the developed techniques. Then, the phases of the methodology (Fig. 1) are disclosed on the sample images acquired from various image surveys. The dynamic thresholding phase for *S* channel is explained in Section 2.2. The phases of the masking and dilation are presented in Section 2.3.

2.1. HSV and its applications in the methodology

The main colour models are RGB, HSV, CIELAB, CMYK, and XYZ. The colour models different from the RGB are employed to realise different objectives because several fundamental issues can not be addressed using the additive RGB colour mode for image segmentation such that it is not viable to get the luminance of the image regarding human perception. For instance, the CIELAB colour space that is close to the human visual perception is applied to H&E stained microscopical images to correct the Kohler illumination problem in microscopical images (Kuru, 2014). Likewise, HSV provides a close representation of human visual perception of colour in cylindrical-coordinate representations as illustrated in *Fig. 4* whereas the RGB colour mode represents the colours processing in the human biological visual system (Loesdau et al., 2014). HSV stands for i) the hue that corresponds to the angle (from the red at $0°$, to the green at $120°$ and the blue at $240°$, and then back to red again at $360°$), more explicitly, moving from red to yellow to green to cyan to blue to magenta and back to red, ii) the saturation that corresponds to the distance from the axis (i.e., radius), the brightness of the colour, and iii) the value indicating the luminance or intensity.

Fig. 2. User interfaces. Left: the main platform developed for multi purpose environmental applications. Right: man–made object detection and splitting interface that can be opened from the main platform.

In HSV, the component, hue, has the most control over the colour information compared to the other components in terms of determining the colour information whereas the saturation designates the colourfulness relative to the brightness based on the amount of light it appears to absorb and how much light it seems to be emitting. The saturation characteristics of ISMMMOs are significantly different from those of the sea background and maritime animals, as explained earlier. Therefore, we process the chromatic hue and saturation components to reveal the artificial objects not belonging to the natural marine environment. First, the hue component is shifted by 180° to suppress the blueish background into reddish (Fig. 4) as shown in the examples in Figs. 11c, 12c, 13c, 14c, 15c and in the technical reports in the supplements. Second, more saturated sections of the image are made more distinctive as explained in Section 2.2.

2.2. Dynamic thresholding in *S* channel

It is observed that the closer the values of histogram *S* are to the centre, with respect to the distribution of histograms, the likelier the pixels are of representing the background and natural marine life, and vice versa the more likelier they represent ISMMMOs wherever these values get away from the axis meaning that saturation is greater. However, there is no specific value that makes this separation distinct based on the different features of the images acquired in different circumstances, mainly different lighting times of the day, month, season, and type of camera. Furthermore, the distribution of the histogram values plays a major role in representing the characteristics of the image regarding the colourfulness relative to the brightness to which to which an area radiate a varying amount of light as explained in Section 1. The objective is to separate more saturated regions from less saturated ones to determine if there is an unnatural object. All threshold values and necessary parameters need to be determined based on the distribution and features of datasets in many surveys

without any user intervention due to the maritime dynamics and image capturing techniques. It is noteworthy to emphasise that the saturation values are almost normally distributed with a Gaussian function as displayed in Eq. 1. The exact distribution of data points using this Gaussian function is presented in Fig. 5 with respect to the σ.

$$P(x) = \frac{1}{\sigma\sqrt{2\pi}}e^{-(x-\mu)^2/2\sigma^2} \qquad (1)$$

In the first instance, a viable threshold value that separates more saturated regions from less saturated ones is found using 145 images with ISMMMOs and 5000 images with no ISMMMOs which were acquired from 22 aerial surveys as shown Fig. 3 I. A ROC curve is an ideal figure to observe how the classification model performs at various classification cut-off points using TPR (True Positive Rate) and FPR (False Positive Rate) (1-TNR) (Table 3). Hence, a ROC curve is established using a large set of threshold values, i.e., cut-off points (i.e., 17) for the
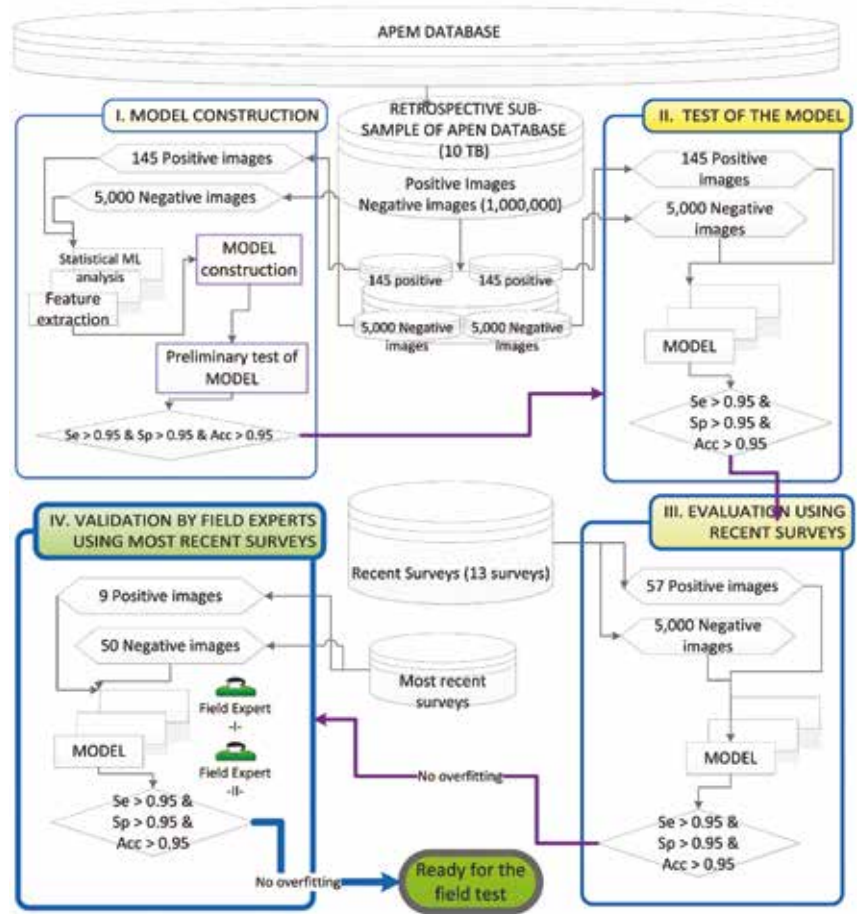

Fig. 3. Use of datasets during model construction, testing, evaluation, and validation of the model.
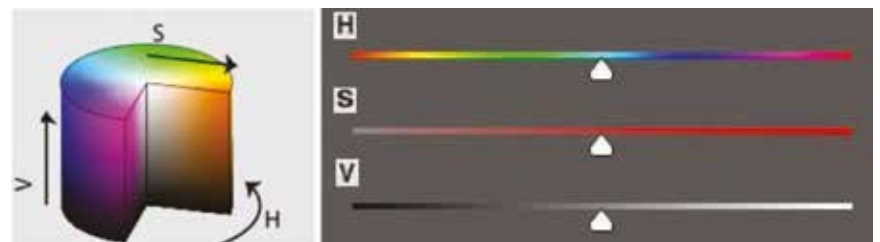

Fig. 4. Model of the HSV colour space. The left image is the courtesy of the author in (Rosebrock, 2017).

purpose of determining the optimal cut-off point, which is the point of the curve nearest to the upper left-hand corner. The results are shown in Table 4. The optimum cut-off point, 0.17, is found, which is between the cut-off points of 0.15 and 0.20 as displayed in *Fig. 6*, and this results in 0.856 (i.e., TP = 124) and 0.817 (i.e., TN = 817) and 0.80 for sensitivity (*Se*), specificity (*Sp*) and accuracy (i.e., *ACC*) respectively. However, these outcomes are far away from our objectives in terms of separating images with ISMMMOs from others within large-scale surveys

with higher accuracy rates. In other words, in order to achieve the desired separation (i.e., (*Se*) > 0.95, *Sp* > 0.95, and *ACC* > 0.95), a curve that is much closer to the top left-hand side of the ROC figure is required where the area under the ROC curve (i.e., AUC) increases, which is a desirable outcome for a test.

The saturation varies significantly, in particular, from one survey to another based on the changing conditions as mentioned above and demonstrated in the technical reports in the supplements with

many examples.[4] Therefore, the designs of various ROC curves are based on the several most important sections of the histogram concerning the distribution of the saturation, and *Se* and *Sp* values by determining the required number of dynamic cut-off points for increasing the Se and Sp values significantly. Technically speaking, i) the mean values (μ) and standard deviations (σ) are acquired following the histogram of the *S* components are obtained from those 145 images mentioned earlier, ii) they are classified based on their μ values and iii)
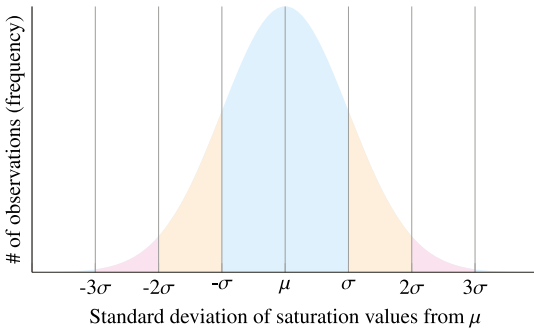
Fig. 5. Generation of the probability distribution using the Gaussian function in Eq. 1 and representation of the standard deviation (σ) of saturation values from μ. Areas: blue (one σ of μ): 0.6826; orange: 0.2718; magenta: 0.0428; sides (right of 3σ and left of –3σ): 0.0027. (For interpretation of the references to colour in this figure legend, the reader is referred to the web version of this article.)
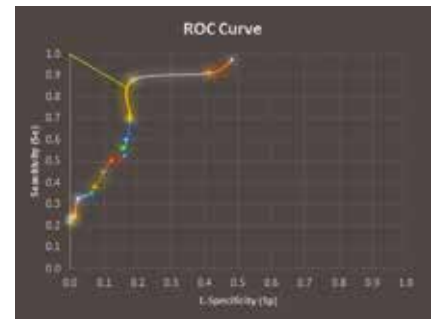

Fig. 6. ROC Curve for Table 4 based on TPR (y-axis) and FPR (x-axis) at 17 classification thresholds: The best cut–off point is 0.17 that is closest to the upper left corner of the curve between the cut–off points 0.15 and 0.20.

Algorithm 1: HSV colour space adjustment function where hAdjust = 0.17 and sAdjustPar = 180.

```
1  FUNCTION newImage = HSVadjustManMade(img, hAdjust,sAdjustMask):
2  − >convert the image from RGB colour space into HSV space;
3  hsvVAL = rgb2hsv(img);
4  hue = 360*hsvVAL(:,:,1);
5  h = hsvVAL(:,:,1); s = hsvVAL(:,:,2); v = hsvVAL(:,:,3);
6  meanS = mean2(s);
7  stdS = std2(s);
8  − >perform the dynamic thresholding for S channel;
9  if meanS > 0.50 then
10     sAdjust = meanS - 2*stdS;
11 else if meanS > 0.25 then
12     sAdjust = meanS - stdS/2;
13 else if meanS > sAdjustMask then
14     sAdjust = meanS;
15 else
16     sAdjust = meanS + 4*stdS;
17 s (s > sAdjust) = 1;
18 − >perform the shifting of H channel;
19 h = (mod(hue + hAdjust, 360)) / 360;
20 − >acquire the updated RGB image from HSV space;
21 hsvVAL(:, :, 1) = h; hsvVAL(:, :, 2) = s; hsvVAL(:, :, 3) = v;
22 newImage = hsv2rgb(hsvVAL);
```
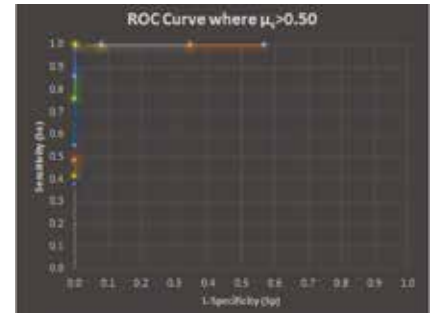

Fig. 7. ROC Curve for Table 5: The best cut–off point is μ – 2σ.
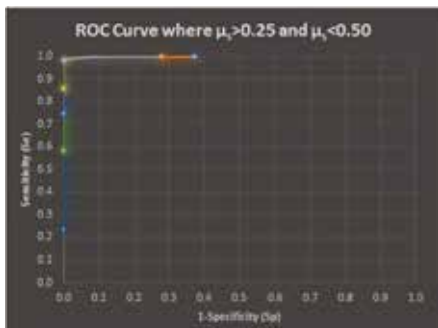
Fig. 8. ROC Curve for Table 6: The best cut–off point is μ – σ/2.

Fig. 9. ROC Curve for Table 7: The best cut–off point is μ.

Fig. 10. ROC Curve for μs where <0.17 (Table 8): The best cut–off point is μ + 4σ.

those classes are analysed separately to find out the best cut-off points for each class. The sections on which the ROC curves are analysed are depicted in Figs. 7, 8, 9, 10 and in Tables 5, 6, 7 and *8* based on the distribution 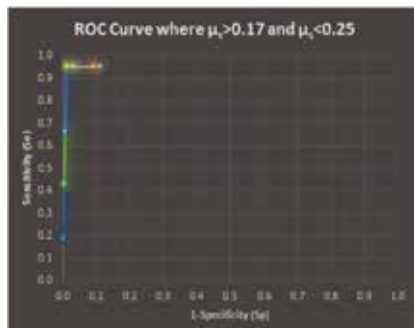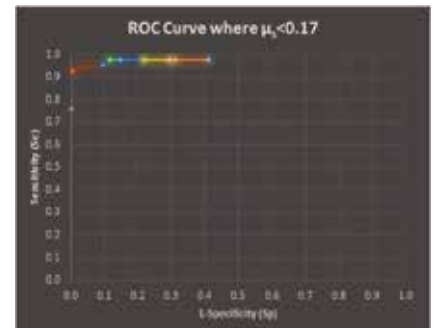of the histogram using the statistical analysis of the μ and σ values where the cut-off points on the ROC curves are specified based on the times of σ in the both directions of μ (Fig. 5).

The number of the cut-off points for each class is specified based on the distribution of the histogram values. This analysis is mainly carried out to find out i) if there is an evident saturated region in the image that distinctively differs from the other majority regions regarding the features of saturation and most importantly ii) what the best cut-off points making this distinction resulting in higher *Se* and *Sp* values are. The histogram values based on the obtained best cut-off points are transformed to the most outer side of the radius in S channel and set to 1 to make the most saturated sections more distinct, in other words, the probable ISMMMOs visible using the masking and dilation techniques mentioned in Section 2.3. Several examples are presented in Figs. 11, 12, 13, 14 and 15. The observed best cut-off points regarding the analysed sections along with their *Se* and *Sp* values in those ROC curves are summarised in *Table 9*. The implementation of dynamic thresholding is presented in Algorithm 1 and exemplified in Figs. 11d, 12d, 13d, 14d, 15d with several examples along with *H* shifting whose new histograms are presented in the second rows of Figs. 11b, 12b, 13b, 14b, 15b.

The methodology was developed using the characteristics and distribution of 22 surveys with around 3 million large-scale images that have been acquired in the various geographical regions, and in the various time zones and seasons. The images with no ISMMMOs were exploited to obtain the general characteristic of the background whereas the images with ISMMMOs were used to determine the general characteristics of ISMMMOs. Both features are merged in the methodology to distinguish the ISMMMOs from its background and consequently discern the positive images from the negative images for further analysis.

2.3. Masking and dilation

Two masks are applied on the image acquired from the dynamic thresholding technique on *H* and *S* channels mentioned above, one of which is for detecting the blueish part and the other one is for removing the unwanted background parts
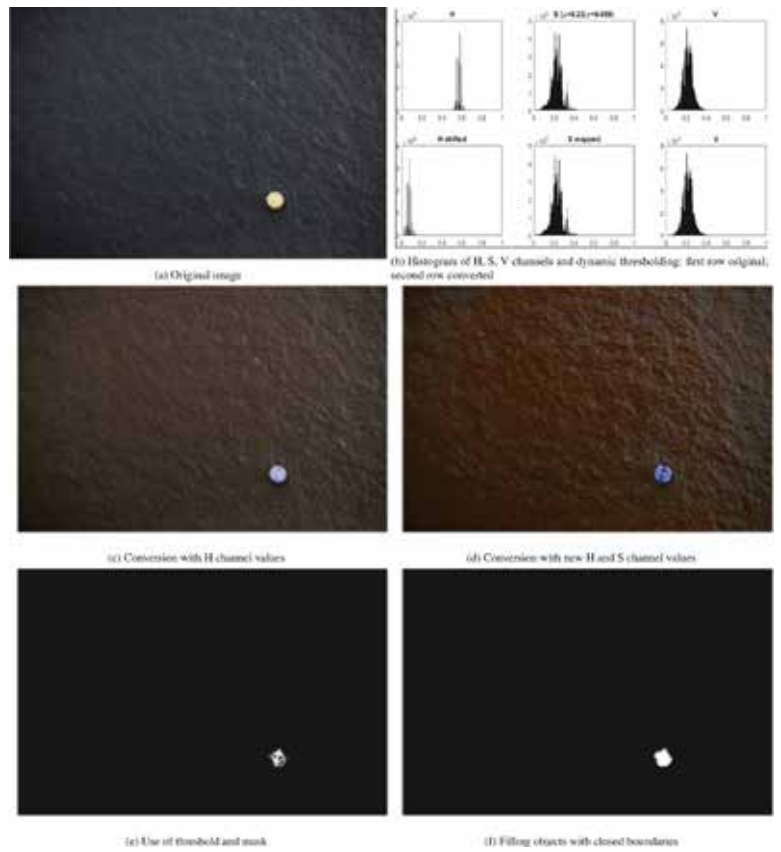

Fig. 11. Stationary example 1: man–made object detection.
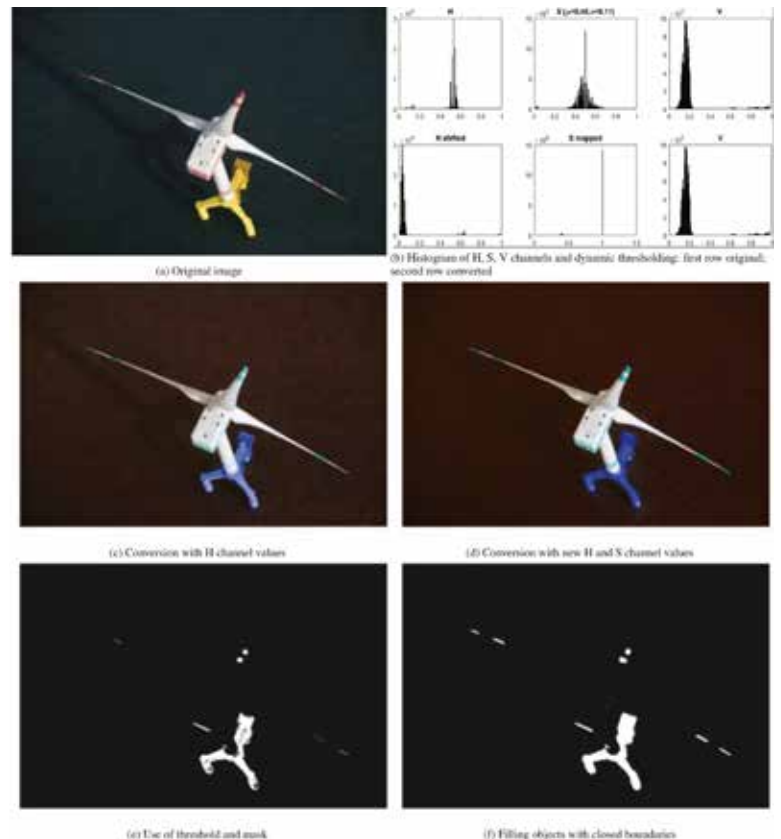
Fig. 12. Stationary example 2: man–made object detection.
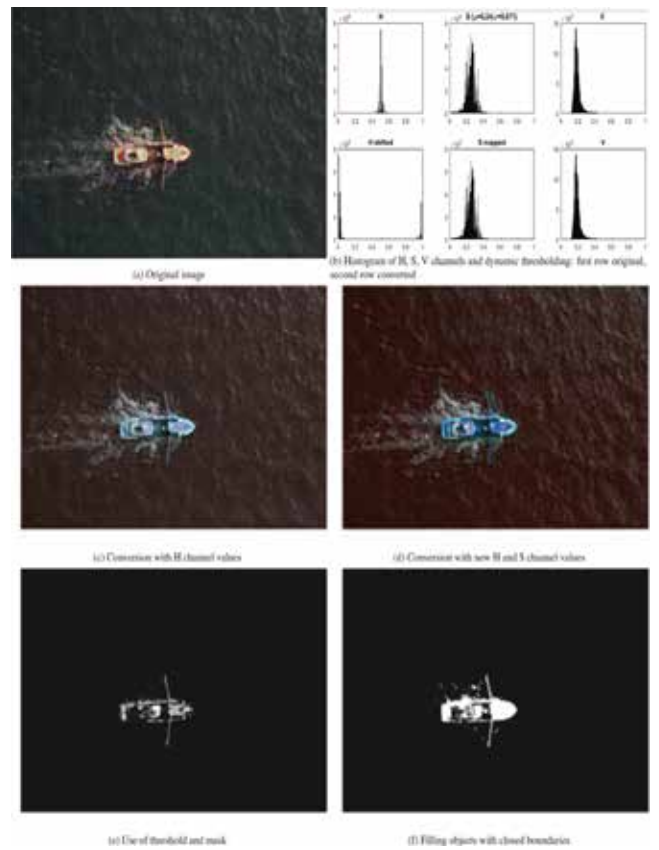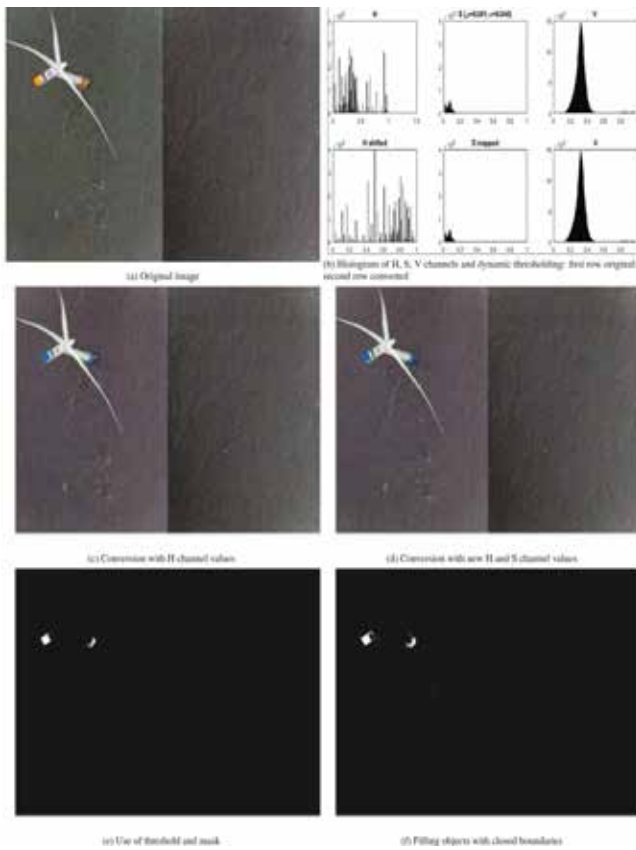
Fig. 13. Stationary example 3: man-made object detection.

Fig. 14. Moving example 1: man-made object detection.

from the image. First mask (i.e.,(($ImgR < 0.25 \& ImgG < 0.80 \& ImgB = 1$) $\& (ImgR < (ImgB) \& ImgG < (ImgB)$))) makes the blueish sections visible by suppressing all other sections, in particular, reddish parts that dominantly indicate the background of sea as depicted in Figs. 11e, 12e, 13e, 14e, 15e and in our technical reports. After applying this mask, the obtained image is dilated and holes are filled to make ISMMMOs coherent as shown in Figs. 11f, 12f, 13f, 14f, 15f. This process is mainly performed to gain the complete white areas of objects that are not obtained with the proposed technique as elaborated in Sections 5 and 7.

There might be several small unwanted dots that are not a part of the ISMMMOs after applying the first mask, usually a process of glinting sections after the HSV processing phase. Around 20% of the blank images come up with similar small dots usually after dilation and filling holes in the image as depicted in Fig. 16h). Several examples for these types of processed images can be reached from our technical report (e.g., examples 4, 6, 7, 15, 17, 19, 20 in MarineObjects_ Man- made_Technical_Blank_1.pdf) in the supplements. These small sections are much smaller than the ISMMMOs and are discarded by applying a size mask technique. In the last phase of the implementation, the images with detected ISMMMOs are labelled as positive images and placed in a separate directory by the application for further analysis.

Fig. 15. Moving example 2: man-made object detection.

Table 1: Formulas for converting from RGB to HSV colour space.

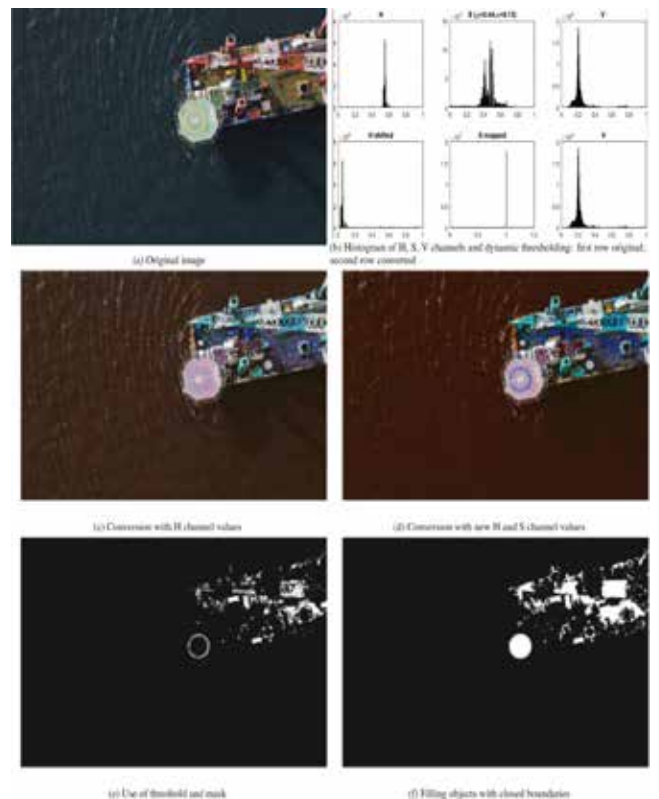| Channel	Formula	Condition / Output	
Rnew	= Red / 255	Output: $0 < Rnew < 1$	Red value mapped between 0 and 1
Gnew	= Green / 255	Output: $0 < Gnew < 1$	Green value mapped between 0 and 1
Bnew	= Blue / 255	Output: $0 < Bnew < 1$	Blue value mapped between 0 and 1
MaxRGB	= Max (Rnew, Gnew, Bnew)	Output: maximum assigned	Maximum of three components found
MinRGB	= Min (Rnew, Gnew, Bnew)	Output: minimum assigned	Minimum of three components found
	= 0	If Rnew = Gnew = Bnew	Zero assigned
Hue (H)	= 60 * ((Gnew - Bnew) / (MaxRGB - MinRGB)) + 0	If max is Rnew	
	= 60 * ((Bnew - Rnew) / (MaxRGB - MinRGB)) + 2	If max is Gnew	Add 360 to Hue if $H < 0$
	= 60 * ((Rnew - Gnew) / (MaxRGB - MinRGB)) + 4	If max is Bnew	
Saturation (S)	= 0	If Rnew = Gnew = Bnew	Zero assigned
	= (MaxRGB - MinRGB) / MaxRGB	Else	If all components different
Value (V)	= MaxRGB	Output: maximum assigned	Maximum of three components assigned

Table 2: Formulas for converting from HSV to RGB colour space.

Channel	Formula	Condition / Output	
Chroma (Chr)	= S * V	Output: Colourfulness	Intermediate colour purity calculated
MidX value	$= Chr(1 - \|(H/60)mod2 - 1\|)$	Output: Mid value	Intermediate conversion value calculated
MidM value	= V - Chr	Output: Mid parameter	Intermediate parameter calculated
	= (Chr, MidX, 0)	If $0 \leq H < 60$	Intermediate red, green and blue calculated based on Hue
	= (MidX, Chr, 0)	If $60 \leq H < 120$	Intermediate red, green and blue calculated based on Hue
(MidR, MidG, MidB)	= (0, Chr, MidX)	If $120 \leq H < 180$	Intermediate red, green and blue calculated based on Hue
	= (0, MidX, Chr)	If $180 \leq H < 240$	Intermediate red, green and blue calculated based on Hue
	= (MidX, 0, Chr)	If $240 \leq H < 300$	Intermediate red, green and blue calculated based on Hue
	= (Chr, 0, MidX)	If $300 \leq H < 360$	Intermediate red, green and blue calculated based on Hue
Rback	= (MidR + MidM) × 255	Output: Targeted red value	Red value calculated using intermediate parameter
Gback	= (MidG + MidM) × 255	Output: Targeted green value	Green value calculated using intermediate parameter
Bback	= (MidX + MidM) * 255	Output: Targeted blue value	Blue value calculated using intermediate parameter

Table 3: Main statistical terms and calculations used throughout the paper.

#	Abbreviation	Description	Detail
1	P	Positive	An image with ISMMMO
2	N	Negative	An image with no ISMMMO
3	TP	True Positive	An image with ISMMMO is tagged as "image with ISMMMO"
4	TN	True Negative	An image without ISMMMO is tagged as "image without ISMMMO"
5	FP	False Positive (False Alarm)	An image without ISMMMO is tagged as "image with ISMMMO"
6	FN	False Negative	An image with ISMMMO is tagged as "image without ISMMMO"
7	Se	Sensitivity	True Positive Rate (TPR) = Se = TP / (TP + FN) How strong is the test in detecting images with ISMMMO correctly.
8	Sp	Specificity	True Negative Rate (TNR) = Sp = TN / (TN + FP) How strong is the test in detecting images without ISMMMO correctly.
9	PPV	Positive Predictive Value	Precision (Pr) = PPV = TP / (TP + FP) How strong is the test in assigning images with ISMMMO to Positive class.
10	NPV	Negative Predictive Value	NPV = TN / (TN + FN) How strong is the test in assigning images without ISMMMO to Negative class.
11	ACC	Accuracy	ACC = (TN + TP) / (FP + FN + TP + TN) Overall correct assignment rate of the test.
12	MCC	Matthews Correlation Coefficient	$MCC = (TN * TP - FN * FP) / \sqrt{((TP+FN)(TP+FP)(TN+FN)(TN+FP))}$ Quality of a test concerning the unbalance in classes
13	μ	Mean	Arithmetic average of a set of observed values.
14	σ	Standard deviation	Measurement of variation, dispersion from the average, within a set of observed values.

Table 4: Finding the optimum point using 17 cut-off points. 145 images with ISMMMOs

Cut-off	TP	FN	TN	FP	Se	Sp	1-Sp
0.05	141	4	517	483	0.972	0.517	0.483
0.10	132	13	585	415	0.910	0.585	0.415
0.15	127	18	814	186	0.876	0.814	0.186
0.20	101	44	821	179	0.697	0.821	0.179
0.25	87	58	832	168	0.600	0.832	0.168
0.30	81	64	841	159	0.559	0.841	0.159
0.35	76	69	835	165	0.524	0.835	0.165
0.40	73	72	877	123	0.503	0.877	0.123
0.45	65	80	901	99	0.448	0.901	0.099
0.50	55	90	927	73	0.379	0.927	0.073
0.55	51	94	932	68	0.352	0.932	0.068
0.60	51	94	936	64	0.352	0.936	0.064
0.65	47	98	977	23	0.324	0.977	0.023
0.70	35	110	988	12	0.241	0.988	0.012
0.75	35	110	997	3	0.241	0.997	0.003
0.80	32	113	1000	0	0.221	1.000	0.000
0.85	32	113	1000	0	0.221	1.000	0.000

Table 5: Statistical analysis using 11 cut-off points: 29 images with ISMMMOs where µs > 0.50.

Cut-off	TP	FN	TN	FP	Se	Sp	1-Sp
$\mu - 5\sigma$	29	0	432	568	1.000	0.398	0.602
$\mu - 4\sigma$	29	0	653	347	1.000	0.653	0.347
$\mu - 3\sigma$	29	0	917	83	1.000	0.917	0.083
$\mu - 2\sigma$	29	0	997	3	1.000	0.997	0.003
$\mu - \sigma$	25	4	999	1	0.862	0.999	0.001
μ	22	7	1000	0	0.759	1.000	0.000
$\mu + \sigma$	16	13	1000	0	0.552	1.000	0.000
$\mu + 2\sigma$	14	15	1000	0	0.483	1.000	0.000
$\mu + 3\sigma$	14	15	1000	0	0.483	1.000	0.000
$\mu + 4\sigma$	12	17	1000	0	0.414	1.000	0.000
$\mu + 5\sigma$	11	18	1000	0	0.379	1.000	0.000

Table 6: Statistical analysis using 7 cut-off points. 55 images with ISMMMOs where µs >0.25 and < 0.50.

Cut-off	TP	FN	TN	FP	Se	Sp	1-Sp
$\mu - 2\sigma$	20	1	887	113	0.952	0.887	0.113
$\mu - \sigma$	20	1	908	92	0.952	0.908	0.092
$\mu - \sigma/2$	20	1	967	33	0.952	0.967	0.033
μ	20	1	987	13	0.952	0.987	0.013
$\mu + \sigma/2$	14	7	993	7	0.667	0.993	0.007
$\mu + \sigma$	9	12	995	5	0.429	0.995	0.005
$\mu + 2\sigma$	4	17	998	2	0.190	0.998	0.002

Table 7: Statistical analysis using 7 cut–off points. 21 images with ISMMMOs where μs > 0.17 and < 0.25.

Cut-off	TP	FN	TN	FP	Se	Sp	1-Sp
$\mu - 2\sigma$	55	0	627	373	1.000	0.627	0.373
$\mu - \sigma$	55	0	721	279	1.000	0.721	0.279
$\mu - \sigma/2$	54	1	998	2	0.982	0.998	0.002
μ	47	8	1000	0	0.855	1.000	0.000
$\mu + \sigma/2$	41	14	1000	0	0.745	1.000	0.000
$\mu + \sigma$	32	23	1000	0	0.582	1.000	0.000
$\mu + 2\sigma$	13	42	1000	0	0.236	1.000	0.000

Table 8: Statistical analysis using 10 cut–off points. 40 images with ISMMMOs where μs < 0.17.

Cut-off	TP	FN	TN	FP	Se	Sp	1-Sp
$\mu - \sigma$	40	1	587	413	0.976	0.587	0.413
$\mu - \sigma/2$	40	1	685	315	0.976	0.685	0.315
μ	40	1	704	296	0.976	0.704	0.296
$\mu + \sigma/2$	40	1	781	219	0.976	0.781	0.219
$\mu + \sigma$	40	1	851	149	0.976	0.851	0.149
$\mu + 2\sigma$	40	1	883	117	0.976	0.883	0.117
$\mu + 3\sigma$	39	2	903	97	0.951	0.903	0.097
$\mu + 4\sigma$	38	3	994	6	0.927	0.994	0.006
$\mu + 5\sigma$	31	10	997	3	0.756	0.997	0.003
$\mu + 6\sigma$	27	14	997	3	0.659	0.997	0.003

Appendix A. Pseudo codes of the methodology based on the Matlab syntax

---

Algorithm 2: Main methodology titled startSplittingObjectsUnsupervised: Phases of the operations to detect man-made objects in images.

Data: The target directory of a survey with images.
Result: Two directories, one of which is for images with man-made objects, and the other is for other images.
1 − >Variables;
2 infoDetail=''; steps = 1; k=1; posImageCount = 0; name = 'Human object detection';
3 set(handles.edtGeneral, 'String', ''); set(handles.edtDetail, 'String', ''); set(h,'Name','WilDetection: Splitting images using unsupervised technique'); set(h, 'Position', [1090 50 355 50]) set(handles.edtGeneral, 'String', strcat(name,' is on process...')); set(handles.edtDetail, 'String', 'The information will be displayed here after the process above is completed.');
4 − >Create NEG and POS folder;
5 [parentFolder deepestFolder] = fileparts(imageDir); negSubFolder = sprintf('%s/NEG-%s', imageDir, deepestFolder); posSubFolder = sprintf('%s/POS-%s', imageDir, deepestFolder);
6 − > Create the folders if they do not exist.;
7 **if** *exist(negSubFolder, 'dir')* **then**
8   mkdir(negSubFolder);

9 **if** *exist(posSubFolder, 'dir')* **then**
10   mkdir(posSubFolder);

11 − > Progress bar to show the progress of the process;
12 h = waitbar(0.1,'Please wait...','CreateCancelBtn',... 'setappdata(gcbf,"canceling",1); delete(gcbf);')
13 − > Start splitting;
14 **[Result,posImageCount] = startSplittingManMadeObjects(imageDir,posSubFolder,handles,h);**
15 infoDetail = strcat(name,' has been completed; Total count of POS images is', ' ', num2str(posImageCount));
16 c_str1=[infoDetail];
17 set(handles.edtDetail, 'String', c_str); set(h,'Name','WilDetection: Splitting process of man-made object detection is COMPLETED');
18 waitbar(k / steps,h,sprintf('COMPLETED'));
19 ImDir = dir([imageDir, '.jpg']);
20 totNegImageCount = length(ImDir(not([ImDir.isdir])));
21 set(handles.edtNegCount, 'String', num2str(totNegImageCount));
22 set(handles.edtGeneral, 'String', ' All tasks have been completed');
23 result = 'Splitting images has been completed.';

Table 9: Dynamic threshold points for S channel based on μ and σ acquired from the statistical analysis of the images using several cut-off points as depicted in Tables 5, 6, 7, 8. The most closest pointi to the upper left corner of the ROC curve indicate the ideal cut-off points as shown in Figs. 7, 8, 9, 10.

Mean of the S channel (μ)	threshold	objective	Se	Sp	example
> 0.50	$\mu - 2x\sigma$	Almost all values are mapped to 1	1.00	0.997	Fig. 16b
> 0.25	$\mu - \sigma/2$	Most of the values are mapped to 1	0.982	0.987	Fig. 12b
> sAdjustMask (i.e, 0.17)	μ	Almost half of the values are mapped to 1	0.927	0.994	Fig. 14b
otherwise (i.e., < 0.17)	$\mu + 4x\sigma$	Most of the values are not mapped to 1, left as is	0.96	0.95	Fig. 13b

End notes

[1] https://apem-inc.com

[2] https://www.apemltd.co.uk

[3] APEM Ltd. is an environmental company and proposes novel solutions for environmental problems (https://www.apemltd.co.uk).

[4] The reports from 1 to 7 titled as MarineObjects_ Man-made_Supplement are for ISMMMOs and the reports from 1 to 5 titled as MarineObjects_Man-made_Supplement_Blank are for blank images.

The paper is republished with authors' permission.To be concluded in next issue.

References

[1] C. E. Elrick-Barr, J. S. Zimmerhackel, G. Hill, J. Clifton, F. Ackermann, M. Burton, E. S. Harvey, Man-made structures in the marine environment: A review of stakeholders' social and economic values and perceptions, Environmental Science & Policy 129 (2022) 12–18. doi:https://doi.org/10.1016/j.envsci.2021.12.006.

[2] Y. Shi, C. Shen, H. Fang, H. Li, Advanced control in marine mechatronic systems: A survey, IEEE/ASME Transactions on Mechatronics 22 (3) (2017) 1121–1131. doi:10.1109/TMECH.2017.2660528.

[3] K. Kuru, H. Yetgin, Transformation to advanced mechatronics systems within new industrial revolution: A novel framework in automation of everything (aoe), IEEE Access 7 (2019) 41395–41415. doi:10.1109/ACCESS.2019.2907809.

[4] S. C. Riser, H. J. Freeland, D. Roemmich, S. Wijffels, A. Troisi, M. Belbéoch, D. Gilbert, J. Xu, S. Pouliquen, A. Thresher, P.-Y. L. Traon, G. Maze, B. Klein, M. Ravichandran, F. Grant, P.-M. Poulain, T. Suga, B. Lim, A. Sterl, P. Sutton, K.-A. Mork, P. J. Velez-Belchí, I. Ansorge, B. King, J. Turton, M. Baringer, S. R. Jayne, Fifteen years of ocean observations with the global argo array, Nature Climate Change 6 (1) (2016) 145–153.

[5] T. Zhang, B. Tian, D. Sengupta, L. Zhang, Y. Si, Global offshore wind turbine dataset, Scientific Data 8 (1) (2021) 191.

[6] M. Paleczny, E. Hammill, V. Karpouzi, D. Pauly, Population trend of the world's monitored seabirds, 1950-2010, PLOS ONE 10 (6) (2015) e0129342. doi:10.1371/journal.pone.0129342.

[7] K. V. Rosenberg, A. M. Dokter, P. J. Blancher, J. R. Sauer, A. C. Smith, P. A. Smith, J. C. Stanton, A. Panjabi, L. Helft, M. Parr, P. P. Marra, Decline of the north american avifauna, Science 366 (6461) (2019) 120–124. doi:10.1126/science.aaw1313.

[8] M. Sànchez-Marrè, U. Cortés, J. Comas, Environmental sciences and artificial intelligence, Environmental Modelling & Software 19 (9) (2004) 761 – 762, environmental Sciences and Artificial Intelligence. doi:https://doi.org/10.1016/j.envsoft.2003.08.009.

[9] C. Bibby, M. Jones, S. Marsden, Expedition Field Techniques: Bird Surveys, Royal Geographical Society, London, 1998.

[10] B. S. McIntosh, G. Alexandrov, K. Matthews, J. Mysiak, M. [van Ittersum], Preface: Thematic issue on the assessment and evaluation of environmental models and software, Environmental Modelling & Software 26 (3) (2011) 245 – 246, thematic issue on the assessment and evaluation of environmental models and software. doi:https://doi.org/10.1016/j.envsoft.2010.08.008.

[11] A. Abu, R. Diamant, Feature set for classification of man-made underwater objects in optical and sas data, IEEE Sensors Journal 22 (6) (2022) 6027–6041. doi:10.1109/JSEN.2022.3148530.

[12] Z. Han, J. Xing, X. Wang, F. Xue, J. Fan, A robust lcse-resnet for marine man-made target classification based on optical remote sensing imagery, International Journal on Artificial Intelligence Tools 31 (06) (2022) 2240022. doi:10.1142/S021821302240022X.

[13] K. Kuru, W. Khan, Novel hybrid object-based non-parametric clustering approach for grouping similar objects in specific visual domains, Applied Soft Computing 62 (2018) 667 – 701. doi:https://doi.org/10.1016/j.asoc.2017.11.007.

[14] K. Kuru, S. Girgin, K. Arda, U. Bozlar, A novel report generation approach for medical applications: The sisds methodology and its applications, International Journal of Medical Informatics 82 (5) (2013) 435–447. doi:https://doi.org/10.1016/j.ijmedinf.2012.05.019.

[15] M. Mehrnejad, A. B. Albu, D. Capson, M. Hoeberechts, Detection of stationary animals in deep-sea video, in: 2013 OCEANS - San Diego, 2013, pp. 1–5. doi:10.23919/OCEANS.2013.6741095.

[16] J. Lopez, J. Schoonmaker, S. Saggese, Automated detection of marine animals using multispectral imaging, in: 2014 Oceans - St. John's, 2014, pp. 1–6. doi:10.1109/OCEANS.2014.7003132.

[17] J. Graber, Land-based Infrared Imagery for Marine Mammal Detection, Master's thesis, University of Washington, USA (2011).

[18] G. Saur, S. Estable, K. Zielinski, S. Knabe, M. Teutsch, M. Gabel, Detection and classification of man-made offshore objects in terrasar-x and rapideye imagery: Selected results of the demarine-deko project, in: OCEANS 2011 IEEE - Spain, 2011, pp. 1–10. doi:10.1109/Oceans-Spain.2011.6003596.

[19] F. S. Leira, T. A. Johansen, T. I. Fossen, Automatic detection, classification and tracking of objects in the ocean surface from uavs using a thermal camera, in: 2015 IEEE Aerospace Conference, 2015, pp. 1–10. doi:10.1109/AERO.2015.7119238.

[20] K. L. Davis, E. D. Silverman, A. L. Sussman, R. R. Wilson, E. F. Zipkin, Errors in aerial survey count data: Identifying pitfalls and solutions, Ecology and Evolution 12 (3) (2022) e8733. arXiv:https://onlinelibrary.wiley.com/doi/pdf/10.1002/ece3.8733, doi:https://doi.org/10.1002/ece3.8733.

[21] N. Clements, W. Robinson, A re-survey of winter bird communities in the oregon coast range, USA, initially surveyed in 1968-1970, Biodiersity Data Journal (Aug. 2022). doi:10.3897/arphapreprints.e91575.

[22] K. Kuru, S. Clough, D. Ansell, J. McCarthy, S. McGovern, Wildetect: An intelligent platform to perform airborne wildlife census automatically in the marine ecosystem using an ensemble of learning techniques and computer vision, Expert Systems with Applications 231 (2023) 120574. doi:https://doi.org/10.1016/j.eswa.2023.120574.

[23] A. Noe, L. Pessoa, E. Thompson, Beyond the grand illusion: what change blindness really teaches us about vision, Visual Cognition 7 (2) (2000) 93–106.

[24] A. Rosebrock, Face alignment with opencv and python (2017) [cited 01.13.2022].
URL http://www.pyimagesearch.com/2017/05/22/face-alignment-with-opencv-and-python/

[25] K. Kuru, Optimization and enhancement of h&e stained microscopical images by applying bilinear interpolation method on lab color mode, Theoretical Biology and Medical Modelling 11 (1) (2014) 9. doi:10.1186/1742-4682-11-9.

[26] M. Loesdau, S. Chabrier, A. Gabillon, Hue and Saturation in the RGB Color Space, Springer International Publishing, Cham, 2014, pp. 203–212. doi:10.1007/978-3-319-07998-1_23.

[27] K. Gibert, J. S. Horsburgh, I. N. Athanasiadis, G. Holmes, Environmental data science, Environmental Modelling & Software 106 (2018) 4 – 12, special Issue on Environmental Data Science. Applications to Air quality and Water cycle. doi:https://doi.org/10.1016/j.envsoft.2018.04.005.

[28] H. Xing, Z. Xiao, D. Zhan, S. Luo, P. Dai, K. Li, Selfmatch: Robust semisupervised time-series classification with self-distillation, International Journal of Intelligent Systems 37 (11) (2022) 8583–8610. doi:https://doi.org/10.1002/int.22957.

[29] Z. Xiao, H. Zhang, H. Tong, X. Xu, An efficient temporal network with dual self-distillation for electroencephalography signal classi-

fication, in: 2022 IEEE International Conference on Bioinformatics and Biomedicine (BIBM), 2022, pp. 1759–1762. `doi:10.1109/BIBM55620.2022.9995049`.

[30] H. Xing, Z. Xiao, R. Qu, Z. Zhu, B. Zhao, An efficient federated distillation learning system for multitask time series classification, IEEE Transactions on Instrumentation and Measurement 71 (2022) 1–12. `doi:10.1109/TIM.2022.3201203`.

[31] A. Çalışkan, Detecting human activity types from 3d posture data using deep learning models, Biomedical Signal Processing and Control 81 (2023) 104479. `doi:https://doi.org/10.1016/j.bspc.2022.104479`.

[32] K. Kuru, D. Ansell, M. Jones, B. J. Watkinson, N. Caswell, P. Leather, A. Lancaster, P. Sugden, E. Briggs, C. Davies, T. C. Oh, K. Bennett, C. De Goede, Intelligent autonomous treatment of bedwetting using non-invasive wearable advanced mechatronics systems and mems sensors: Intelligent autonomous bladder monitoring to treat ne, Medical & Biological Engineering & Computing 58 (5) (2020) 943–65. `doi:10.1007/s11517-019-02091-x`.

[33] K. Kuru, et al., Iotfauav: Intelligent remote monitoring of livestock in large farms using autonomous uninhabited aerial vehicles, Computers and Electronics in Agriculture (2023).

[34] K. Kuru, D. Ansell, B. Jon Watkinson, D. Jones, A. Sujit, J. M. Pinder, C. L. Tinker-Mill, Intelligent automated, rapid and safe landmine and unexploded ordnance (uxo) detection using multiple sensor modalities mounted on autonomous drones, IEEE Transactions on Geoscience and Remote Sensing (2023).

[35] K. Kuru, A. Sujit, D. Ansell, J. M. Pinder, B. Jon Watkinson, D. Jones, R. Hamila, C. Tinker-Mill, Iintelligent, automated, rapid, and safe landmine, improvised explosive device and unexploded ordnance detection using maggy, IEEE Access (2024).

[36] K. Kuru, Platform to test and evaluate human-in-the-loop telemanipulation schemes for autonomous unmanned aerial systems, in: IEEE/ASME MESA 2024 – 20th Int. Conference on Mechatronic, Embedded Systems and Applications, 2024.

[37] K. Kuru, Technical report: Analysis of intervention modes in human-in-the-loop (hitl) teleoperation with autonomous unmanned aerial systems, Central Lancashire online Knowledge (2024).

[38] K. Kuru, Human-in-the-loop telemanipulation schemes for autonomous unmanned aerial systems, in: 2024 4th Interdisciplinary Conference on Electrics and Computer (INTCEC), 2024, pp. 1–6. `doi:10.1109/INTCEC61833.2024.10603071`.

[39] K. Kuru, O. Erogul, C. Xavier, Autonomous low power monitoring sensors, Sensors 21 (2021).

[40] K. Kuru, D. Ansell, D. Jones, B. Watkinson, J. M. Pinder, J. A. Hill, E. Muzzall, C. Tinker-Mill, K. Stevens, A. Gardner, Intelligent airborne monitoring of livestock using autonomous uninhabited aerial vehicles, in: The 11th European Conference on Precision Livestock Farming, 2024.

[41] K. Kuru, Use of autonomous uninhabited aerial vehicles safely within mixed air traffic, in: Proceedings of Global Conference on Electronics, Communications and Networks (GCECN2024), 2023.

[42] K. Kuru, Technical report: Essential development components of the urban metaverse ecosystem, Central Lancashire online Knowledge (2024).

[43] K. Kuru, Technical report: Analysis of intervention modes in human-in-the-loop (hitl) teleoperation with autonomous ground vehicle systems, Central Lancashire online Knowledge (2022).

[44] K. Kuru, Metaomnicity: Toward immersive urban metaverse cyberspaces using smart city digital twins, IEEE Access 11 (2023) 43844–68. `doi:10.1109/ACCESS.2023.3272890`.

[45] K. Kuru, Sensors and sensor fusion for decision making in autonomous driving and vehicles (2023).

[46] K. Kuru, Telemanipulation of autonomous drones using digital twins of aerial traffic, IEEE Dataport (2024). `doi:10.21227/kn5m-z290`.

[47] K. Kuru, A Novel Hybrid Clustering Approach for Unsupervised Grouping of Similar Objects, Springer International Publishing, 2014, p. 642–653. `doi:10.1007/978-3-319-07617-1_56`.

[48] K. Kuru, Optimization and enhancement of h&e stained microscopical images by applying bilinear interpolation method on lab color mode, Theoretical Biology and Medical Modelling 11 (1) (2014). `doi:10.1186/1742-4682-11-9`.

[49] K. Kuru, Definition of multi-objective deep reinforcement learning reward functions for self-driving vehicles in the urban environment, IEEE Trans. Veh. Technol. 11 (2024) 1–12.

[50] K. Kuru, Management of geo-distributed intelligence: Deep insight as a service (DINSaaS) on forged cloud platforms (FCP), Journal of Parallel and Distributed Computing 149 (2021) 103–118. `doi:10.1016/j.jpdc.2020.11.009`.

[51] K. Kuru, D. Ansell, Tcitysmartf: A comprehensive systematic framework for transforming cities into smart cities, IEEE Access 8 (2020) 18615–18644. `doi:10.1109/ACCESS.2020.2967777`.

[52] K. Kuru, K. Kuru, Urban metaverse cyberthreats and countermeasures to mitigate them, in: Proceedings of IEEE Sixth International Conference on Blockchain Computing and Applications (BCCA 2024), 2024.

[53] K. Kuru, Conceptualisation of human-on-the-loop haptic teleoperation with fully autonomous self-driving vehicles in the urban environment, IEEE Open J. Intell. Transp. Syst. 2 (2021) 448–69. `doi:10.1109/OJITS.2021.3132725`.

[54] K. Kuru, J. M. Pinder, B. J. Watkinson, D. Ansell, K. Vinning, L. Moore, C. Gilbert, A. Sujit, D. Jones, Toward mid-air collision-free trajectory for autonomous and pilot-controlled unmanned aerial vehicles, IEEE Access 11 (2023) 100323–100342. `doi:10.1109/ACCESS.2023.3314504`.

[55] K. Kuru, Planning the future of smart cities with swarms of fully autonomous unmanned aerial vehicles using a novel framework, IEEE Access 9 (2021) 6571–6595. `doi:10.1109/ACCESS.2020.3049094`.

[56] K. Kuru, W. Khan, A framework for the synergistic integration of fully autonomous ground vehicles with smart city, IEEE Access 9 (2021) 923–948. `doi:10.1109/ACCESS.2020.3046999`.

[57] K. Kuru, Trustfsdv: Framework for building and maintaining trust in self-driving vehicles, IEEE Access 10 (2022) 82814–82833. `doi:10.1109/ACCESS.2022.3196941`.

[58] K. Kuru, D. Ansell, W. Khan, H. Yetgin, Analysis and optimization of unmanned aerial vehicle swarms in logistics: An intelligent delivery platform, IEEE Access 7 (2019) 15804–31. `doi:10.1109/ACCESS.2019.2892716`.

[59] K. Kuru, K. Kuru, Blockchain-enabled privacy-preserving machine learning authentication with immersive devices for urban metaverse cyberspaces, in: 2024 20th IEEE/ASME International Conference on Mechatronic and Embedded Systems and Applications (MESA), 2024, pp. 1–8. `doi:10.1109/MESA61532.2024.10704877`.

[60] K. Kuru, B. J. Watkinson, D. Ansell, D. Hughes, M. Jones, N. Caswell, P. Leather, K. Bennett, P. Sugden, C. Davies, C. DeGoede, Smart wearable device for nocturnal enuresis, in: 2023 IEEE EMBS Special Topic Conference on Data Science and Engineering in Healthcare, Medicine and Biology, 2023, pp. 95–96. `doi:10.1109/IEEECONF58974.2023.10404506`.

[61] K. Kuru, Technical report: Big data-concepts, infrastructure, analytics, challenges and solutions (2024).

[62] K. Kuru, D. Ansell, D. Hughes, B. J. Watkinson, F. Gaudenzi, M. Jones, D. Lunardi, N. Caswell, A. R. Montiel, P. Leather, D. Irving, K. Bennett, C. McKenzie, P. Sugden, C. Davies, C. Degoede, Treatment of nocturnal enuresis using miniaturised smart mechatronics with artificial intelligence, IEEE Journal of Translational Engineering in Health and Medicine 12 (2024) 204–214. `doi:10.1109/JTEHM.2023.3336889`.

[63] K. Kuru, M. Niranjan, Y. Tunca, Establishment of a diagnostic decision support system in genetic dysmorphology, in: 2012 11th International Conference on Machine Learning and Applications, Vol. 2, 2012, pp. 164–169. `doi:10.1109/ICMLA.2012.234`.

[64] J. Lowe, K. Kuru, Design & development of a smart blind system using fuzzy logic, in: 2024 20th IEEE/ASME International Conference on Mechatronic and Embedded Systems and Applications (MESA), 2024, pp. 1–8. `doi:10.1109/MESA61532.2024.10704868`.

[65] J. Lowe, K. Kuru, Development of machine intelligence for self-driving vehicles through video capturing, in: 2024 20th IEEE/ASME International Conference on Mechatronic and Embedded Systems and Applications (MESA), 2024, pp. 1–8. `doi:10.1109/MESA61532.2024.10704876`.

[66] K. Kuru, S. Worthington, D. Ansell, J. M. Pinder, A. Sujit, B. Jon Watkinson, K. Vinning, L. Moore, C. Gilbert, D. Jones, et al., Aitl-wing-hitl: Telemanipulation of autonomous drones using digital twins of aerial traffic interfaced with wing, Robotics and Autonomous Systems 180 (2024).

[67] K. Kuru, K. Kuru, Urban metaverse cyberspaces & blockchain-enabled privacy-preserving machine learning authentication with immersive devices, in: Proceedings of IEEE Sixth International Conference on Blockchain Computing and Applications (BCCA 2024), 2024.

[68] K. Kuru, K. Kuru, Urban metaverse cybercommunities & blockchain-based privacy-preserving deep learning authentication and verification with immersive metaverse devices, in: Proceedings of IEEE Sixth International Conference on Blockchain Computing and Applications (BCCA 2024), 2024.

[69] K. Kuru, K. Kuru, Urban metaverse cyberthreats and countermeasures against these threats, in: Proceedings of IEEE Sixth International Conference on Blockchain Computing and Applications (BCCA 2024), 2024.

[70] K. Kuru, S. Girgin, K. Arda, U. Bozlar, V. Akgün, Developing Diagnostic DSSs Based on a Novel Data Collection Methodology, Springer Berlin Heidelberg, 2009, p. 110–121. `doi:10.1007/978-3-642-10488-6_14`.

[71] K. Kuru, S. Girgin, K. Arda, A Novel Multilingual Report Generation System for Medical Applications, Springer Berlin Heidelberg, 2009, p. 201–205. `doi:10.1007/978-3-642-02976-9_29`.

[72] K. Kuru, A novel report generation system for medical applications (2009).

[73] K. Kuru, M. Niranjan, Y. Tunca, E. Osvank, T. Azim, Biomedical visual data analysis to build an intelligent diagnostic decision support system in medical genetics, Artificial Intelligence in Medicine 62 (2) (2014) 105–118. `doi:10.1016/j.artmed.2014.08.003`.

[74] K. Kuru, W. Khan, Novel hybrid object-based non-parametric clustering approach for grouping similar objects in specific visual domains, Appl. Soft Comput. 62 (2018) 667–701.

[75] K. Kuru, S. Clough, D. Ansell, J. McCarthy, S. McGovern, Wildetect: An intelligent platform to perform airborne wildlife census automatically in the marine ecosystem using an ensemble of learning techniques and computer vision, Expert Systems with Applications 231 (2023) 120574. `doi:10.1016/j.eswa.2023.120574`.

[76] K. Kuru, S. Clough, D. Ansell, J. McCarthy, S. McGovern, Intelligent airborne monitoring of irregularly shaped man-made marine objects using statistical machine learning techniques, Ecological Informatics 78 (2023) 102285. `doi:10.1016/j.ecoinf.2023.102285`.

[77] K. Kuru, Joint cognition of remote autonomous robotics agent swarms in collaborative decision-making & remote human-robot teaming, Proceedings of The Premium Global Conclave and Expo on Robotics & Automation (AUTOROBO, EXPO2024) (2024).

[78] N. Caswell, K. Kuru, D. Ansell, M. J. Jones, B. J. Watkinson, P. Leather, A. Lancaster, P. Sugden, E. Briggs, C. Davies, C. Oh, K. Bennett, C. DeGoede, Patient engagement in medical device design: Refining the essential attributes of a wearable, pre-void, ultrasound alarm for nocturnal enuresis, Pharmaceutical Medicine 34 (1) (2020) 39–48. `doi:10.1007/s40290-019-00324-w`.

[79] K. Kuru, D. Ansell, M. Jones, C. De Goede, P. Leather, Feasibility study of intelligent autonomous determination of the bladder voiding need to treat bedwetting using ultrasound and smartphone ml techniques: Intelligent autonomous treatment of bedwetting, Medical & Biological Engineering & Computing 57 (5) (2018) 1079–1097. `doi:10.1007/s11517-018-1942-9`.

[80] K. Kuru, S. Girgin, K. Arda, U. Bozlar, A novel report generation approach for medical applications: The sisds methodology and its applications, International Journal of Medical Informatics 82 (5) (2013) 435–447. `doi:10.1016/j.ijmedinf.2012.05.019`.

[81] K. Kuru, K. Kuru, Blockchain-based decentralised privacy-preserving machine learning authentication and verification with immersive devices in the urban metaverse ecosystem (2024). `doi:10.20944/preprints202402.0317.v1`.

[82] K. Kuru, S. Girgin, A Bilinear Interpolation Based Approach for Optimizing Hematoxylin and Eosin Stained Microscopical Images, Springer Berlin Heidelberg, 2011, p. 168–178. `doi:10.1007/978-3-642-24855-9_15`.

[83] K. Kuru, Use of wearable miniaturised medical devices with artificial intelligence (ai) in enhancing physical medicine, Proceedings of Enhancing Physical Medicine. In: World Congress on Physical Medicine and Rehabilitation (2024).

[84] K. Kuru, A. Sujit, D. Ansell, J. M. Pinder, D. Jones, B. Watkinson, R. Hamila, C. L. Tinker-Mill, Non-invasive detection of landmines, unexploded ordnances and improvised explosive devices using bespoke unmanned aerial vehicles, Proceedings of EEE International Conference on Electrical and Computer Engineering Researches (ICECER'24) (2024).

[85] K. Kuru, Technical report: Towards state and situation awareness for driverless vehicles using deep neural networks, Central Lancashire online Knowledge (2024).

[86] K. Kuru, Technical report: Human-in-the-loop telemanipulation platform for automation-in-the-loop unmanned aerial systems, Central Lancashire online Knowledge (2024).

[87] K. Kuru, S. Clough, D. Ansell, J. McCarthy, S. McGovern, Wildetect-part i, Coordinates 20 (5) (2024) 19–29.

[88] K. Kuru, S. Clough, D. Ansell, J. McCarthy, S. McGovern, Wildetect-part ii, Coordinates 20 (6) (2024) 17–25.

[89] K. Kuru, S. Clough, D. Ansell, J. McCarthy, S. McGovern, Intelligent airborne monitoring of irregularly shaped man-made marine objects using statistical machine learning techniques, Ecological Informatics 78 (2023) 102285. `doi:10.1016/j.ecoinf.2023.102285`.